

pubs.acs.org/cm Article

Microporous Pentiptycene-Based Polymers with Heterocyclic Rings for High-Performance Gas Separation Membranes

Zihan Huang, Claire Yin, Tanner Corrado, Si Li, Qinnan Zhang, and Ruilan Guo*



Cite This: Chem. Mater. 2022, 34, 2730-2742



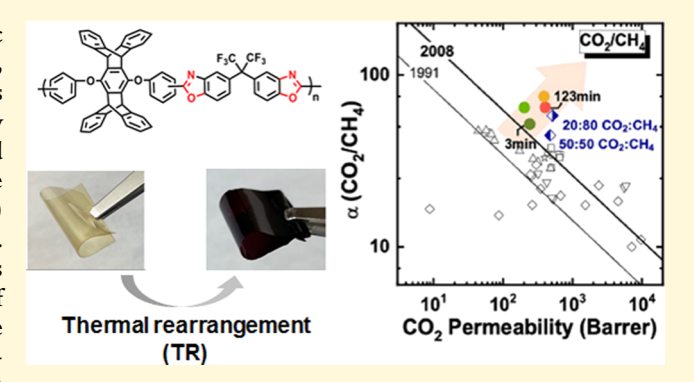
ACCESS

Metrics & More

Article Recommendations

s Supporting Information

ABSTRACT: Microporous polymers, such as polymers of intrinsic microporosity (PIMs) and thermally rearranged (TR) polymers, have shown promise in advancing the performance of polymer gas separation membranes to overcome the permeability—selectivity trade-off. In this work, a series of thermally rearranged pentiptycene-based polybenzoxazole (PPBO) polymers were prepared from a new pentiptycene-based poly(o-hydroxyl imide) (PPHI) precursor using carefully designed thermal protocols. Fundamental structure—property relationships within the series were established by comprehensively examining the effects of intermediate treatment temperature and the heating rate on the membrane microporosity, properties, and gas separation performance. The incorporation of bulky pentiptycene units into TR PPBO



structures, along with optimized TR thermal protocols in this study, provided a route to finely tune and eventually maximize the separation performance of PPBOs, with several films far exceeding the 2015 upper bound for H_2/CH_4 and O_2/N_2 . In CO_2/CH_4 mixed-gas permeation tests, PPBO membranes showed excellent resistance to plasticization under CO_2 partial pressure as high as 6.6 atm, far surpassing the 2008 mixed-gas upper bound for CO_2/CH_4 . Moreover, a 5 month aged PPBO film maintained its superior separation performance above the 2008 O_2/N_2 upper bound and 2015 H_2/CH_4 upper bound, indicating the excellent aging resistance of PPBOs.

1. INTRODUCTION

Since the 1970s, membrane-mediated gas separation technologies have been growing phenomenally for various separation processes such as air separation (O_2/N_2) , hydrogen recovery $(H_2/N_2, H_2/CH_4, \text{ and } H_2/CO_2)$, and natural gas purification (CO_2/CH_4) . Compared with conventional thermally driven separation technologies, such as cryogenic distillation, polymeric membrane-mediated gas separation processes are enormously energy-efficient, easy to maintain, cost-effective, and environmentally friendly with small footprints.^{2,4-8} However, the trade-off relationship between permeability and selectivity represents one of the major challenges faced by polymer membranes, which is empirically plotted as "upper-bound" lines in permeability vs. selectivity plots.^{2,9} In the past few decades, guided by a general macromolecular design principle that suggests large interchain spacing and high polymer backbone rigidity, numerous new polymers have been developed and investigated to address the challenge of permeability-selectivity trade-off. Among these endeavors, two classes of polymers, i.e., polymers with intrinsic microporosity (PIMs) and thermally rearranged (TR) polymers, have emerged with highly promising and attractive gas separation performance.^{2,10} PIMs belong to a class of ladder polymers fabricated from hierarchical monomers with fused aromatic rings and highly contorted configuration (e.g.,

spirocenter). PIMs' highly rigid and inefficiently packed (semi)ladder-like backbone allows for high fractional free volume (FFV), thus ultrahigh permeability, 11-13 which helps define the 2015 upper bounds for O_2/N_2 , H_2/CH_4 , and H_2/N_2 separations as well as the 2019 upper bounds for CO₂/CH₄ and CO₂/N₂. ^{14,15} TR polymers, featuring rigid-rod backbones with benzoxazole-based heterocyclic rings, are fabricated from solution-processable polyimide precursors with ortho-functionality (e.g., -OH group) through solid-state thermal rearrangement process. 16-18 They also demonstrate ultrahigh permeabilities due to the formation of a large number of free volume microcavities during the solid-state imide-to-benzoxazole thermal conversion.¹⁹ While PIMs and TR polymers demonstrate superior separation performance surpassing the upper bound, such improvement predominantly originates from their ultrahigh permeability, and their size-sieving

Received: December 7, 2021 Revised: February 25, 2022 Published: March 8, 2022





Scheme 1. Synthesis of PPDAn Dianhydride Monomer

capability (i.e., selectivity) is much less attractive, mainly due to the lack of finely tuned microporosity.

One of the recent and arguably most effective strategies to improve the selectivity of PIMs and TR polymers is to introduce shape-persistent building blocks or structural units with intrinsic molecular microporosity, such as iptycene moieties, to boost the size-sieving capability. 6,7,20-22 Iptycenes are [2,2,2]-ring systems composed of fused aromatic rings, with the simplest configurations being triptycene and pentiptycene, containing three and five arene rings, respectively.²³ Providing internal free volume (IFV) elements intrinsic to the molecular configurations that have dimensions comparable to the kinetic diameters of many gas molecules, iptycene units have been proven to be capable of generating finely tailored free volume architecture, therefore enabling superior size-sieving properties. 7,24-27 Previous study in our group has successfully demonstrated the first iptycenecontaining TR polymers, i.e., triptycene-based PBOs (TPBOs), showing superior separation performance exceeding the 2015 H₂/CH₄ upper bound and the CO₂/CH₄ and O₂/N₂ 2008 upper bounds, representing arguably the most selective TR polymers.^{21,28}

Here, pentiptycene units are introduced for the first time as the building block to prepare a series of microporous PBObased TR polymer membranes to further explore the potential of iptycene-containing TR polymers for gas separation applications. As a natural extension to triptycene, bulkier pentiptycene unit, composed of five arene rings fused in a Hshape scaffold, can disrupt chain packing more efficiently once introduced into the PBO backbone, leading to higher permeability than its triptycene counterparts, as demonstrated in our previous studies on pentiptycene-based polyimides /,2/,2/ and pentiptycene-PIM.²⁰ Furthermore, pentiptycene has a higher fraction of IFV elements, which will not only augment the overall free volume but also improve further the sizesieving behavior of the TR membranes, enabling higher permeability-selectivity combinations. In this study, a series of thermally rearranged pentiptycene-based PBO (PPBO) polymers were prepared from a new pentiptycene-based poly(o-hydroxyl imide) (PPHI) precursor following systematically varied TR thermal treatment protocols. Fundamental structure-property relationships within the series were established by comprehensively examining the effects of intermediate treatment temperature and the heating rate on

the membrane microporosity, properties, and gas separation performance. Mixed-gas permeation performance and physical aging resistance were also investigated on the PPBO films. We demonstrate that the microporosity and gas transport properties of PPBOs can be feasibly and finely tailored by applying different thermal protocols, which, when optimized, led to superior separation performance surpassing existing TR polymers.

2. EXPERIMENTAL SECTION

2.1. Materials. Anthracene (Alfa Aesar, 97%), *p*-benzoquinone (Sigma-Aldrich, ≥98%), 4-nitrophthalonitrile (TCI, >980%), toluene (>99.5%, Sigma-Aldrich), *m*-cresol (>99%, Alfa Aesar), and isoquinoline (>97%, Sigma-Aldrich) were used as purchased without further purifications. 2,2′-Bis(3-amino-4-hydroxyphenyl)hexafluoropropane (6FAP, >98.5%), purchased from Akron Polymer systems, was dried at 65 °C under vacuum before polymerization. *N*-Methyl-2-pyrrolidone (NMP, ≥98%), dimethyl sulfoxide (DMSO, ≥99.9%), and anhydrous *N*,*N*-dimethylformamide (DMF, 99.8%) were purchased from Sigma-Aldrich. All other chemicals were purchased from commercial sources without further purification.

2.2. Synthesis of Pentiptycene-Based Dianhydride Monomer (PPDAn). Synthesis of pentiptycene-based dianhydride monomer (PPDAn) was modified from the protocols reported previously for triptycene-based dianhydride monomer (TPDAn) synthesis³⁰ and is shown in Scheme 1. A typical synthesis is as follows: the pentiptycene diol, PENT-OH, was first synthesized following previously reported procedures. ^{27,31,32} In a two-neck round-bottom flask connected with a constant N₂ flow, PENT-OH (4.0 g, 8.6 mmol) and 4-nitrophthalonitrile (3.1 g, 17.7 mmol) were reacted in anhydrous DMF (28 mL) under the presence of anhydrous potassium carbonate (K₂CO₃, 2.5 g, 17.7 mmol) at room temperature for 24 h. The obtained crude pentiptycene-based tetranitrile product, PENT-4CN, was washed in methanol and water mixture (300:300 mL) three times and further purified by refluxing in excessive DMSO (350 mL) at 190 °C for 36 h. Once the heat was removed, a hot filtration was performed immediately on the refluxed dispersion to avoid the precipitation of impurities upon cooling. The high-purity and white PENT-4CN powder product (78% yield) was collected and further dried in the vacuum oven at 100 °C overnight. To hydrolyze PENT-4CN to the corresponding tetracarboxylic acid, PENT-4COOH: under a N2 flow, PENT-4CN (4.8 g, 6.7 mmol) and potassium hydroxide (KOH, 19.1 g, 1.1 mmol) were completely dissolved and reacted in DMSO/water mixture (95:95 mL/mL) for at least 72 h at 130 °C. The ammonia content in the reaction exhaust was checked constantly with a water-damped pH paper. In this reaction, the presence of DMSO greatly enhanced the solubility and conversion of

hydrolysis. Upon the completion of the reaction where no change in the color of pH paper was observed, the clear solution containing deprotonated PENT-4COOH product was collected. To the collected solution, 6 M hydrochloride (HCl) was added dropwise till pH was about 1.0. The precipitated and protonated PENT-4COOH (90% yield) was collected from filtration and dried in a 100 °C vacuum oven overnight. PPDAn was obtained by refluxing PENT-4COOH (4.7 g, 6.0 mmol) in the acetic anhydride/acetic acid mixture (33: 33 mL) for 9 h at 142 °C under a N₂ flow, which was cooled, filtered, and rinsed with excessive petroleum ether, followed by drying in a vacuum oven at 180 °C overnight. The final PPDAn monomer had a yield of over 70% and high purity. ¹H NMR (500 MHz, DMSO- d_6): δ 5.57 (s, 4H), 6.90-6.92 (m, 8H), 7.16-7.18 (m, 8H), 7.21-7.24 (m, 2H), 7.29-7.30 (d, 2H), 8.12-8.14 (d, 2H). ¹H NMR spectra of PENT-4CN, PENT-4COOH, and the final PPDAn monomers are included in Figures S1-S3.

2.3. Synthesis of *Ortho*-Hydroxyl Pentiptycene Polyimide Precursor (PPHI). The obtained PPDAn was polymerized with 6FAP diamine via condensation polymerization to yield pentiptycenecontaining poly(*o*-hydroxyimide) (PPHI) precursor, shown in Scheme 2a. The polymerization was conducted in *m*-cresol through

Scheme 2. (a) Synthesis of PPHI Precursor and (b) Thermal Rearrangement (TR) of PPHI to PPBO via Imideto-Benzoxazole Conversion

Pentiptycene-based Polybenzoxazole (PPBO)

in situ solution imidization. The procedures are as follows: to a flamed dried three-neck flask coupled with a N2 inlet, a condenser, a Dean-Stark trap, and a mechanical stirrer, 6FAP (0.4889 g, 1.3 mmol) was first added and stirred vigorously in m-cresol (2.4 mL) at room temperature. Next, a stoichiometric amount of PPDAn (1.000 g, 1.3 mmol) was added along with additional m-cresol (10.0 mL) at a total solid content of 10.7% (wt/vol). The mixture was gradually heated to 200 °C and held for 3.5 h until all PPDAn dissolved when the catalytic amount of isoquinoline (0.2 mL) and a small amount of toluene (<1 mL) were added to the reaction flask and the attached Dean-Stark trap was filled with toluene to azeotropically remove the water generated during polycondensation. The thermal imidization was allowed to complete in 5 h at 200 °C, after which the solution was naturally cooled to room temperature and precipitated into the methanol-water (v/v = 1/1, 600 mL) solution. The fibrous PPHI polymer (Figure S4a) was filtered and rinsed with excessive methanol

and dried in a vacuum oven at 180 °C overnight. 1H NMR (500 MHz, DMSO- d_6): δ 5.58 (s, 4H), 6.88 (s, 8H), 7.01–7.03 (d, 4H), 7.17(s, 8H), 7.27–7.30 (d, 4H), 7.43 (s, 2H), 7.93–7.95 (d, 2H), 10.57 (s, 2H).

2.4. Film Casting of PPHI Precursor and Thermal Rearrangement. PPHI thin films with a thickness of $\sim 55-60~\mu m$ were cast using the solution casting method, where PPHI was fully dissolved in NMP ($\sim \! 7\%$ wt/vol, g/mL), filtered through a 0.45 μm PTFE syringe filter, and cast onto a clean and leveled glass plate. A free-standing film was formed by allowing slow evaporation of the solvent under an IR lamp (Staco Energy Products Co., 120 V) overnight at $\sim 65~^{\circ} C$. The film was peeled off from the glass plate and dried in a vacuum oven at 180 $^{\circ} C$ for 48 h to remove the residual solvent. Gas permeation properties of the precursor PPHI film will be reported in a separate study.

Thermal rearrangement (TR) of PPHI precursor films (Scheme 2b) to corresponding PPBO films was performed in a muffle furnace (Thermolyne Type 479) preheated to 100 °C and equipped with a constant N2 flow. PPHI film was sandwiched in between two porous ceramic plates during the TR treatment. Once the temperature stabilized at 100 °C after placing the film, a 10 °C/min heating rate was applied to the desired $T_{\rm g}$ -dependent intermediate isotherm temperature (300 or 350 °C). After holding at the intermediate temperature for 2 h, a predetermined heating rate (10, 30, or 50 °C/ min) was applied to ramp to the final TR temperature, 450 °C, and maintained for another 0.5 h. In cases where no intermediate thermal treatment was applied, the PPHI film was directly ramped to 450 °C at a heating rate of either 10 or 50 °C/min. After the TR process, the furnace was allowed to naturally cool down to ambient conditions with a cooling rate no larger than 10 °C/min. Through varying the intermediate isotherm temperature (2 h duration) and heating rate to a final TR temperature of 450 °C (0.5 h duration), a total of seven PPBO films were obtained, which allowed for a comprehensive examination of the effect of heating protocol on gas transport properties in PPBO films. The obtained PPBO films were named to reflect the thermal protocol from which they were prepared. For example, TR-300-30-450 refers to a PPBO film that was prepared by applying an isothermal treatment at 300 °C for 2 h before ramping at 30 °C/min to a final TR temperature of 450 °C for 0.5 h. The PPBO film samples had an average thickness of 45-55 μ m, each with thickness variation less than 5%, measured by a digital micrometer.

2.5. Characterization Methods. The ¹H NMR spectra of the synthesized PPDAn monomer and PPHI precursor polymer were obtained from a Bruker AVANCE III HD 500 MHz spectrometer in deuterated solvents like CDCl₃ and DMSO-d₆. Attenuated total reflection Fourier transform infrared spectra (ATR-FTIR) of PPHI precursor films and thermally converted PPBO films were recorded from a JASCO FTIR 6300 spectrometer with a resolution of 4 cm⁻¹ and 64 scans. Differential scanning calorimetry (DSC) analysis was performed using DSC Q2000 (TA Instruments) in two heating cycles, where the first cycle was run to 450 °C and the second cycle from 100 to 450 °C, with 10 °C/min and 20 °C/min of heating and cooling rates, respectively, for both cycles. Thermogravimetric analysis (TGA) was operated on TGA Q500 (TA Instruments) at a heating rate of 10 °C/min applied from 100 to 800 °C under a 50 mL/min N₂ purge.

Wide-angle X-ray scattering (WAXS) was performed on all of the PPBO films using a Bruker Advance Davinci X-ray diffractometer. Reflection mode by Cu $K\alpha$ radiation (wavelength, $\lambda=1.54$ Å) was selected, with the current and voltage of the X-ray generator set to 40 kV and 40 mA, respectively. In 2θ ranging from 5 to 45°, a step increment of 0.02° and a scan speed of 7 s per step were assigned for all measurements. The observed diffraction peak maxima at θ (°) were used to calculate the average d-spacing, d (Å), for each film, according to Bragg's law, $d=\lambda/2\sin(\theta)$.

The density of PPBO films was determined at room temperature in deionized (DI) water from an analytical balance (ML204, Mettler Toledo) coupled with a density kit. DI water was chosen due to its negligible absorption in hydrophobic PPBOs. The determination of density is governed by the buoyancy method, and the averaged density value over at least eight measurements was reported.

Chemistry of Materials Article pubs.acs.org/cm

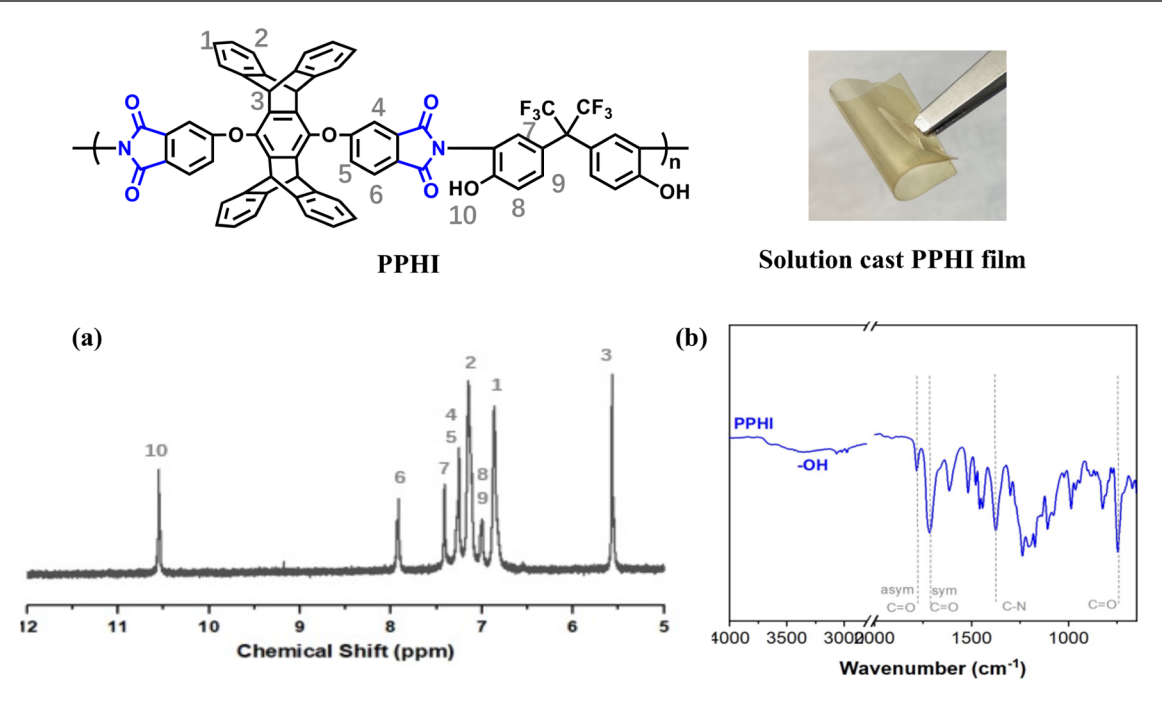


Figure 1. (a) ¹H NMR and (b) ATR-FTIR spectrum of the PPHI precursor.

Fractional free volume (FFV) of the films was then calculated using the following equation

$$FFV = \frac{V_0 - 1.3V_w}{V_0}$$

where V_0 , the molar volume of the polymer film, was calculated based on the experimentally determined density, and V_{wt} the van der Waals volume, was derived from Bondi's group contribution method. 33,34

Ultra-high-purity (UHP) gases (H2, CH4, N2, O2, and CO2) were used in gas permeation tests for all of the PPBO films. The measurements were performed at 35 °C based on the constant volume/variable pressure method.35, Each film was completely degassed overnight before the permeability measurement of each gas. Pure-gas permeabilities were recorded at three upstream pressures (2.1, 9.0, and 15.9 atm) once the downstream pressure accumulation reached steady-state increment, as indicated by a transducer. Permeability is therefore calculated as in the following

$$P = 10^{10} \frac{V_{\rm d}l}{P_{\rm up}TRA} \left[\left(\frac{\rm d}{p} \right)_{\rm ss} - \left(\frac{\rm d}{p} \right)_{\rm leak} \right]$$

P is gas permeability in Barrer (1 Barrer = 10^{-10} cm³(STP)cm/(cm² s cmHg)), V_d (cm³) is the total volume of downstream, l (cm) and A(cm²) are the average film thickness and film area of the test sample, respectively, $P_{\rm up}$ (cmHg) is the absolute upstream pressure, R is gas constant $(0.278 \text{ cm}^3 \text{ cmHg/(cm}^3(\text{STP})\text{K}))$, T(K) is the temperature for pure-gas permeation test, and $(dp/dt)_{ss}$ and $(dp/dt)_{leak}$ are the steady-state increment of permeant pressure accumulated in the downstream and leak rate of downstream under vacuum, respectively. Permeability measurement was repeated on multiple samples for all of the films to ensure reliable results.

The ideal selectivity $(\alpha_{A/B})$ of a given gas pair is calculated by the ratio of pure-gas permeability of the more permeable gas to the other

$$\alpha_{A/B} \equiv \frac{P_A}{P_B}$$

The apparent diffusion coefficient, D (cm²/s), was calculated from the time-lag method, as in the following equation

$$D = \frac{l^2}{6\theta}$$

where θ is the lag time (s).

Solubility, S, is therefore calculated based on the solution—diffusion model by

$$S = \frac{P}{D}$$

The mixed-gas permeation tests on the CO₂/CH₄ gas pair at 35 °C were performed through the apparatus of constant pressure/variable volume.³⁵ Binary CO₂:CH₄ gas feeds in two feed compositions, 50:50 and 20:80 molar ratios, were used in mixed-gas permeation measurements under three total feed pressures (6.8, 10.2, and 12.2 atm) for each feed composition. The stage-cut was less than 0.5%, with a total feed flow rate of 200 cm³(STP)min⁻¹. A gas chromatograph (3000 Micro GC, Inficon Inc., Syracuse, NY) and a thermal conductivity detector were used to measure the permeate gas compositions. The permeability of gas A in a binary mixed-gas permeation measurement was calculated by the following equation

$$P_{A} = \frac{x_{A}Sl}{x_{\text{sweep}}A(P_{2,A} - P_{1,A})}$$

where x_A and x_{sweep} are the mole fraction of component A and sweep gas (He), respectively, S is the flow rate of the sweep gas, and $P_{2,A}$ and $P_{1,A}$ are the partial pressure of gas component A in the feed stream and permeate side, respectively. The mixed-gas selectivity of the gas pair was taken as the ratio between the mixed-gas permeability of one gas and that of the other gas.

3. RESULTS AND DISCUSSION

3.1. Synthesis of PPDAn Monomer and PPHI Precursor. We here report a high-yield and high-purity synthesis procedure of PPDAn dianhydride monomer (Scheme 1), which started with Diels-Alder cycloaddition between anthracene and p-benzoquinone. The formed pentiptycene quinone was reduced to pentiptycene diol (PENT-OH) and further substituted by 4-nitrophthalonitrile through the nucleophilic aromatic substitution (S_NAr) reaction. Next, tetranitrile-substituted pentiptycene (PENT-4CN) went

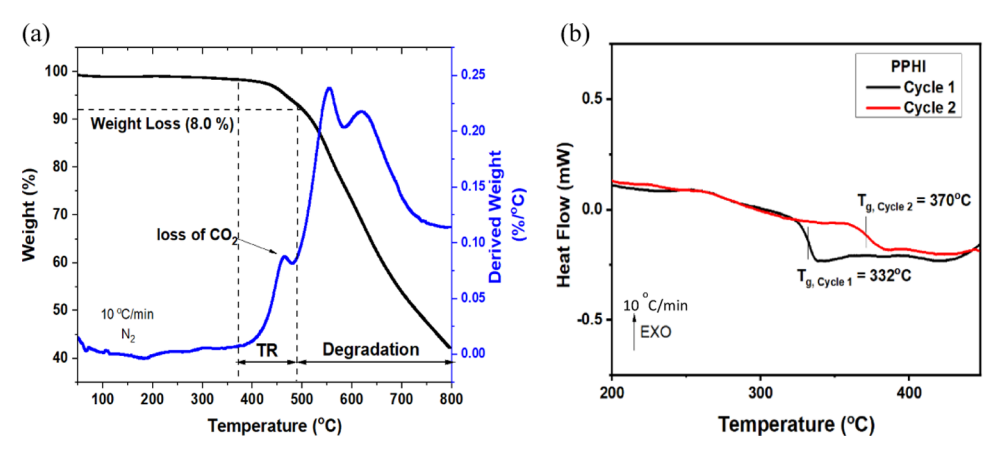


Figure 2. (a) TGA profile of PPHI (10 $^{\circ}$ C/min, N_2) and (b) DSC of PPHI in two heating cycles.

through hydrolysis by potassium hydroxide in the aqueous phase to form pentiptycene tetracarboxylic acid (PENT-4COOH), which was further dehydrated to the final monomer, PPDAn. ¹H NMR spectra of pentiptycene intermediates (Figures S1 and S2) and final PPDAn (Figure S3) demonstrate high purity that allowed successful condensation polymerization to produce the PPHI precursor polymer in high molecular weight.

The obtained PPDAn was polymerized with a commercially available diamine, 6FAP, to yield pentiptycene-containing poly(o-hydroxyimide) (PPHI) following Scheme 2a following a one-step polycondensation reaction in m-cresol at 200 °C under the catalytic amount of isoquinoline. m-cresol was used in this polymerization instead of other common solvents such as NMP because it could more feasibly dissolve PPDAn and consequently afford higher-molecular-weight PPHI. An optimal polymerization concentration of 10.7% wt/vol was identified, which consistently produced high-molecular-weight polymers with high yields as indicated by the fibrous products (Figure S4a) and ensuing robust PPHI films cast from NMP solution. The high-purity and fully imidized structure of PPHI was confirmed by its ¹H NMR and ATR-FTIR spectra (Figure 1). As shown in Figure 1a, all peaks can be unambiguously assigned according to the repeat unit structure of PPHI. For example, the characteristic bridgehead proton of pentiptycene moieties is at 5.59 ppm and the ortho-hydroxyl peak at 10.57 ppm. Similarly, the ATR-FTIR spectrum of the PPHI film shows a broad -OH group peak at 3670 cm⁻¹, indicating that PPHI was functionalized with ortho-hydroxyl groups that enable ensuing thermal rearrangement process to produce the final PPBO membranes. Characteristic imide carbonyl stretching at 1784 cm⁻¹ (C=O asymmetric stretching) and 1717 cm⁻¹ (C=O symmetric stretching), imide C-N stretching at 1378 cm⁻¹, and imide carbonyl (C=O) bending at 720 cm⁻¹ were observed, and no peak was detected for the carbonyl group stretching of the intermediate poly(amic acid), confirming fully imidized structure of PPHI.

3.2. Thermal Properties of PPHI Precursor Film. Thermogravimetric analysis (TGA) is an effective method to characterize thermal rearrangement (TR) conversion of the PPHI precursor, wherein PPHI is thermally converted to PPBO under high temperatures in an inert atmosphere. During TR, *ortho*-hydroxyl groups in PPHI react with the adjacent imide carbonyl groups to generate a mixture of *meta* or *para* linked PBO structures, while releasing CO₂, featured as a region of TR-related weight loss in the TGA profile. ^{18,36,38} In

this study, TGA was performed on PPHI to confirm the occurrence of TR and to identify the optimal TR protocol to be implemented for PPBO film preparation. As seen in Figure 2a, two stages of weight loss can be observed from the TGA pattern. The derivative weight loss with respect to temperature showed the first weight loss region ranging from about 375 to 480 °C with a peak temperature at ~460 °C, characterizing the decarboxylation process during the TR conversion to PPBO, shown in Scheme 2b. The corresponding weight loss in this region is equivalent to the theoretical weight loss (8.0 wt %) of PPHI by the TR process, featuring the release of two CO₂ molecules per repeat unit in PPHI upon thermal conversion. The second stage of weight loss represents the thermal degradation of the thermally converted PPBO, starting from ~485 °C. Compared with the previously reported triptycenecontaining poly(o-hydroxyimide) (TPHI), PPHI has a higher TR peak temperature by ~40 °C, ²¹ indicating higher rigidity of the pentiptycene-based polymer backbone.

Glass-transition temperature (T_g) , an indication of chain flexibility of precursor polymer for TR, is a determinant factor on the efficiency of TR conversion since imide-to-benzoxazole conversion occurs in the solid state. In this regard, TR conversion has to be conducted above the $T_{\rm g}$ of poly(ohydroxyimide) precursors to ensure high imide-to-benzoxazole conversion. 18,38-40 As shown in the DSC profile (Figure 2b), an obvious Tg appeared at about 332 °C in the first heating cycle, indicating a highly rigid PPHI backbone. There is also a broad endothermic peak observed at the tail part of the first heating cycle starting from 400 °C, indicating the occurrence of the TR process. An increased $T_{\rm g}$ of ~370 °C (due to the presence of the partially converted PPBO after ramping to 450 °C in cycle 1) as well as a smaller endothermic peak was observed in the second heating cycle, which, in combination with the TGA profile of PPHI, confirmed the TR-able nature of PPHI precursor.

3.3. Thermal Protocols for TR Conversion of PPHI to PPBO. TR mechanism involves decarboxylation at high-heat treatment (usually > 400 °C) depending on the chain rigidity of the precursor under an inert atmosphere. For TR protocols, parameters like the final TR temperature (e.g., 350–450 °C) and treatment time at TR temperature (e.g., 30 min to 1 h) are commonly practiced to tune TR membrane properties. Other parameters critical to successful TR conversions include an intermediate isothermal treatment usually at around 300 °C for full imidization and complete solvent removal before the TR conversion and the heating rate

to the final TR temperature. $^{44-49}$ However, the values for these two parameters varied from study to study, and especially the intermediate temperature has been hardly related with the intrinsic thermal properties, such as $T_{\rm g}$ of precursor polymer, considering the TR process occurs in solid-state films. As a result, even though the separation performances of different TR polymers were compared against each other quite often, the impact of thermal treatment routes has been barely highlighted in those comparisons.

To fill this fundamental knowledge gap, this study investigates the $T_{\rm g}$ -dependent intermediate treatment temperatures on the separation performance of final PPBO films. Specifically, this study investigated the effect of two key parameters in TR thermal protocols: the intermediate temperature of the 2 h isothermal treatment and the heating rate applied from the intermediate temperature to the final TR temperature ($T_{\rm TR}$). The detailed seven different thermal protocols and corresponding PPBO films are summarized in Table 1. Two intermediate isotherm temperatures were picked

Table 1. Summary of the PPBO Films Prepared from Various Thermal Protocols

starting temperature (°C)	intermediate 2 h isotherm (°C)	heating rate (°C/min)	TR 0.5 h isotherm (°C)	PPBO films
100 ^a	none	10	450 ^b	TR-10-450
		50		TR-50-450
	300	10		TR-300-10-450
		30		TR-300-30-450
		50		TR-300-50-450
	350	10		TR-350-10-450
		50		TR-350-50-450

 a The heating rate is 10 $^{\circ}$ C /min from 100 $^{\circ}$ C to the intermediate isotherm temperature. b 30 min at 450 $^{\circ}$ C for full TR conversion.

using PPHI precursor's $T_{\rm g}$ as a reference: 300 °C (sub- $T_{\rm g}$ temperature), reflecting the conventional intermediate temperature used in the literature, and 350 $^{\circ}$ C (above- $T_{\rm g}$ temperature). 21,37,44 Another parameter in the heating protocol study is the heating rate applied after the 2 h intermediate isotherm to the final $T_{\rm TR}$: slow (10 °C/min), moderate (30 °C/min), or fast (50 °C/min). Direct heating protocols, where either slow or fast heating rate was applied in a thermal treatment directly from 100 °C to the TR temperature (450 °C) without the 2 h intermediate isotherm treatment, were included as well. Different heating rates are expected to affect the chain/ segmental dynamics of the precursor polymer that dictates the efficiency of TR conversion and consequent separation performance. In all cases, a final TR treatment of 0.5 h at 450 °C was applied to keep consistency and ensure full PBO conversion. This final treatment condition was previously established in triptycene-based TPBOs, which showed minimal thermal degradation in TPBOs, while providing the best separation performance compared to that treated at lower T_{TR} for a longer time (e.g., TPBO-450-0.5 h performed better than TPBO-400-1 h).²⁸ In all cases, full TR conversion from PPHI to PPBO by different heating protocols was confirmed by ATR-FTIR spectra (Figure S5), which observed the complete disappearance of the hydroxyl group from the PPHI precursor and the emergence of benzoxazole bands (1561 cm⁻¹, C=N; 1048 cm⁻¹, C-O), though PBO signals are usually weak due to the stable nature of the benzoxazole structure. 21,28,30 The

obtained PPBO films were mechanically robust (Figure S4b), which could sustain a bending angle at more than 90° without fracture and could withstand up to at least 16 bar total feed pressure (the highest pressure of our permeation testing system) in gas permeation tests.

3.4. Effect of Heating Rate on Microporosity and Gas Permeation. The effect of heating rate, i.e., slow (10 °C/min), moderate (30 °C/min), and fast (50 °C/min), on the separation performance of PPBOs was investigated for various gas pairs (Table S1), including H₂/CH₄ (Figure 3a-c), O₂/N₂ (Figure S6), and CO₂/CH₄ (Figure S7). Fundamental gas transport properties of PPBOs were also evaluated in terms of diffusivity and solubility coefficients, as summarized in Table S3 and Figure S8. Correspondingly, microporous structures resulting from different heating rates were examined via the analysis of polymer fractional free volume (FFV) and chain packing (in the form of *d*-spacing by WAXS), as shown in Figure 3d–f and Table S1.

In the case where no intermediate isothermal treatment was applied (Figures 3a, S6a, and S7a), slow heating rate simultaneously improved permeability and selectivity. For example, TR-10-450 (slow heating) showed a close to 2-fold higher H₂ permeability and H₂/CH₄ selectivity than TR-50-450 (fast heating), surpassing the 2015 upper bound for H₂/ CH₄. It has been proposed that during the TR process, small microcavities in TR-able precursors will coalesce and rearrange to hourglass-shaped microcavities with narrow neck regions, which results in much improved permeability and selectivity. 64,65 Since TR conversion occurs effectively only at temperatures above $T_{\rm g}$, the slow heating protocol allows a longer period of the above- $T_{\rm g}$ treatment in the TR-10-450 sample, which greatly enhanced segmental motion essential for TR and likely facilitated the formation of hourglass-shaped micropores. As shown in Figure 3d, TR-10-450 demonstrated both larger average d-spacing (9.83 Å) and FFV (22.3%) than those of TR-50-450 (9.32 Å and 18.0%), supporting higher permeabilities in the TR-10-450 film. Fundamental analysis of diffusivity coefficients (Figure S8 and Table S3) showed that the TR-10-450 film has smaller diffusivities for large gas molecules (e.g., N₂ and CH₄) than the TR-50-450 film. This observation seems to suggest the formation of hourglassshaped microcavities with narrow bottlenecks, explaining the higher selectivity of TR-10-450 than of TR-50-450.

In the case where a 2 h sub- $T_{\rm g}$ (300 °C) intermediate isothermal treatment was applied affording TR-300-10-450, TR-300-30-450, and TR-300-50-450 PPBO films, a similar trend of increasing selectivity with the slower heating rate was observed, where the TR-300-10-450 film (slow heating) was nearly 7 times more selective than the TR-300-50-450 film (fast heating) for H₂/CH₄ (Figure 3b) and similarly for other gas pairs (Figures S6b and S7b). In this series of PPBO films, while heating rate seems to have less impact on permeabilities, moderately decreased permeabilities were observed as slower heating rates were applied. This is likely due to more extensive $\operatorname{sub-}T_{\mathfrak{g}}$ annealing associated with slow heating protocols that led to more densified chain packing, as similarly observed in other glassy polymers. 66,67 The decreased permeability as a result of more densified packing from longer sub- T_{σ} annealing is also evidenced in the decreased d-spacing from 9.79 Å (TR-300-50-450) to 9.58 Å (TR-300-10-450) and FFV from 21.8 to 18.7% as in Figure 3e. The gas diffusivities are also consistent with the trend of permeability of the three films (Figure S8 and Table S3).

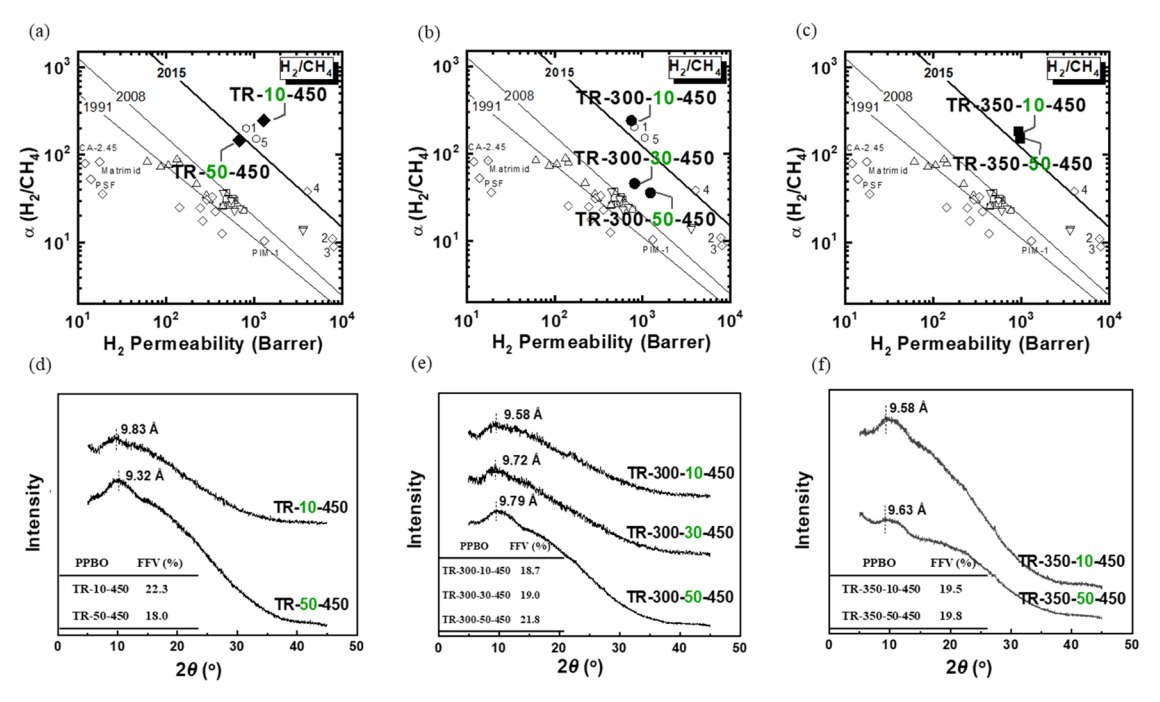


Figure 3. Effect of heating rate on H_2/CH_4 pure-gas performance and microstructure for PPBOs treated by direct heating: (a) and (d); by sub- T_g isotherm: (b) and (e); and by above- T_g isotherm: (c) and (f). The H_2/CH_4 performance is compared against the following reference materials: aPBO (stars), ⁴¹ cross-linked PBOs (squares), ^{50,51} PBO-PI copolymers (triangles), ^{52,53} ortho-polymide derived PBOs (down-triangles), ^{45,54} PIM-PBOs (diamonds), ^{55,56} Matrimid, ⁵⁷ polysulfone (PSF), ⁵⁸ cellulose acetate (CA-2.45), ⁵⁹ PIM-1, ⁶⁰ 1-TPBO, ²¹ Troger's base PIMs (2-PIM-EA-TB, ¹² 3-PIM-Trip-TB⁶¹), and triptycene-based PIMs (4-KAUST-PI-1, ⁶² 5-TPIM-1⁶³).

In the case where an above- $T_{\rm g}$ (350 °C) intermediate isothermal treatment was applied yielding TR-350-10-450 and TR-350-50-450 PPBO films, slow or fast heating rate generated very minimal performance differences for PPBO films though the slowly treated PPBO film (TR-350-10-450) possessed higher selectivity and smaller permeability than the fast-treated TR-350-50-450 film (Figure 3c). For example, H₂ permeability differs by only 3% and CH₄ permeability varies by 17% between TR-350-50-450 and TR-350-10-450 (Table S2), and both films performed above the 2015 H₂/CH₄ upper bound (Figure 3c). A similar performance trend was also observed in O₂/N₂ (Figure S6c) and CO₂/CH₄ separations (Figure S7c). Expectedly, very similar d-spacing and FFV values around 9.6 Å and 20% were observed in the two PPBOs (Figure 3f), which also share very similar diffusivity coefficients (Table S3). These results suggest that the effect of heating rate diminishes when an above- T_g intermediate isothermal treatment is applied. The long enough above- $T_{\rm g}$ treatment in both cases seemed to greatly promote the TR process and formation of hourglass-shaped cavities, leading to superior separation performance surpassing the upper bounds.

3.5. Effect of Intermediate Isotherm Temperature on Microporosity and Gas Permeation. The effect of intermediate isotherm temperature, i.e., 300 °C (sub- T_g) and 350 °C (above- T_g), was examined for PPBO films on their microporosity and separation performances for H_2/CH_4 (Figure 4), O_2/N_2 (Figure S9), and CO_2/CH_4 (Figure S10), and the full permeation data is also summarized in Table S2.

Between the two slowly treated samples shown in Figure 4a, higher intermediate temperature led to moderately increased permeability and decreased selectivity in the TR-350-10-450 film as compared to those in the TR-300-10-450 film though both films are positioned above the 2015 $\rm H_2/CH_4$ upper bound. This is corroborated by the similarly high $\it d$ -spacing

and FFV values demonstrated by the two PPBO films (Figure 4c), in trend with the $\rm H_2$ permeability. The slightly higher selectivity in TR-300-10-450 can be ascribed to the formation of tighter chain packing induced by sub- $T_{\rm g}$ annealing at 300 °C, which is also evidenced by its noticeably lower gas diffusivities than all other PPBOs (Figure S8 and Table S3). On the other hand, the above- $T_{\rm g}$ treatment tends to provide higher gas permeabilities.

Between the two fast-treated samples shown in Figure 4b, a different trend was observed, where the film subjected to the above- T_g intermediate isothermal treatment, TR-350-50-450, showed significantly higher H₂/CH₄ selectivity and similarly high H₂ permeability as compared to the TR-300-50-450 film prepared from the sub- T_{g} intermediate isothermal treatment. This trend was also observed in O_2/N_2 (Figure S9b) and CO_2/N_2 CH₄ (Figure S10b), which is in accordance with their dspacing and FFV values shown in Figure 4d. Analysis of fundamental transport properties showed that the significantly higher selectivity in the TR-350-50-450 sample originated from its markedly lower diffusivities of large gas molecules like N₂ and CH₄ than that in the TR-300-50-450 film (Figure S8 and Table S3). These results further demonstrate the effectiveness of the above- $T_{\rm g}$ treatment in tuning microstructure profiles for enhanced size-sieving capability and high gas throughput.

Based on all of the above discussions, it seems that sufficient heating at a temperature above $T_{\rm g}$ is critical for PPBOs reaching superior separation performance, particularly ultrahigh selectivity (Figure S11). In this regard, the actual above- $T_{\rm g}$ heating time, defined as the exposure time of PPHI to temperatures above $T_{\rm g}$ (332 °C) and below $T_{\rm TR}$ (450 °C) noted as $t_{T_{\rm g}{\rm TR}}$, was used in the evaluation of the synergistic effect of heating rate and intermediate temperature on gas separation performance (Table S1). Permeability and selectivity of all seven PPBO films prepared from different

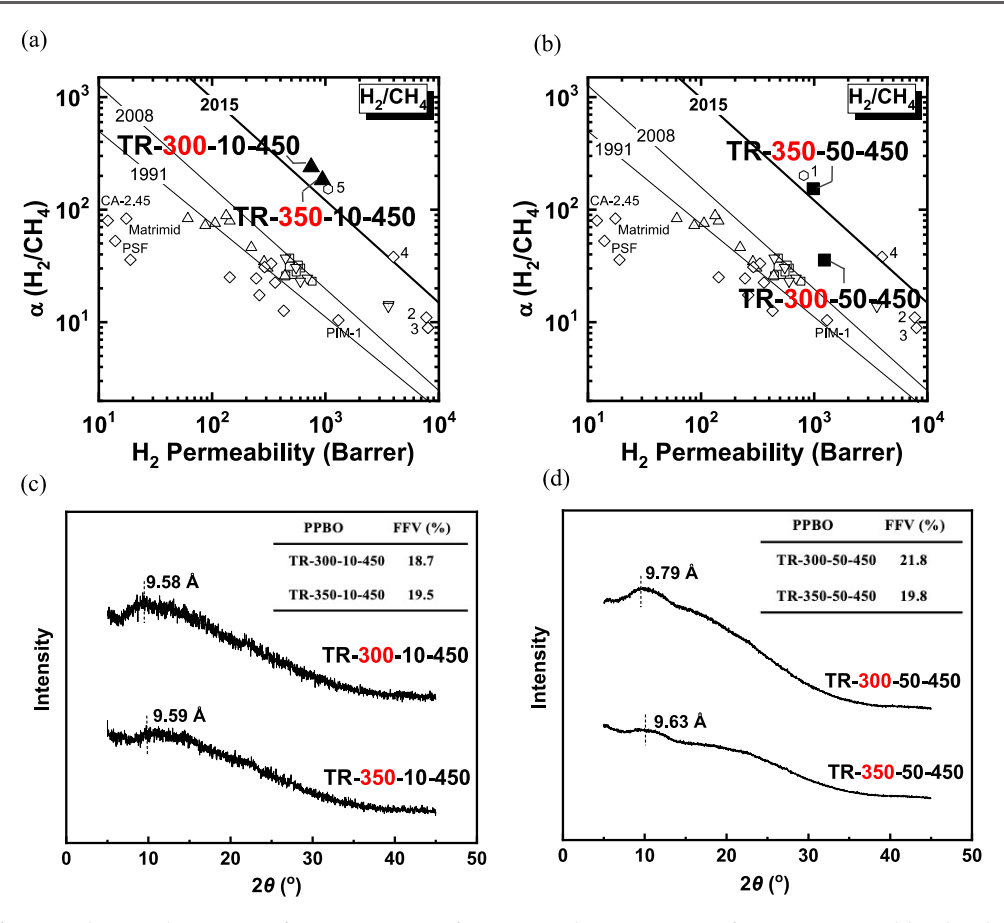


Figure 4. Effect of intermediate isotherm on H₂/CH₄ pure-gas performance and microstructure for PPBOs treated by slow heating rate, 10 °C/min: (a) and (c); by fast heating rate, 50 °C/min: (b) and (d). The H₂/CH₄ performance is compared against the following reference materials: aPBO (stars), ⁴¹ cross-linked PBOs (squares), ^{50,51} PBO-PI copolymers (triangles), ^{52,53} *ortho*-polyimide-derived PBOs (down-triangles), ^{45,54} PIM-PBOs (diamonds), ^{55,56} Matrimid, ⁵⁷ polysulfone (PSF), ⁵⁸ cellulose acetate (CA-2.45), ⁵⁹ PIM-1, ⁶⁰ 1-TPBO, ²¹ Troger's base PIMs (2-PIM-EA-TB, ¹² 3-PIM-Trip-TB⁶¹), and triptycene-based PIMs (4-KAUST-PI-1, ⁶² 5-TPIM-1⁶³).

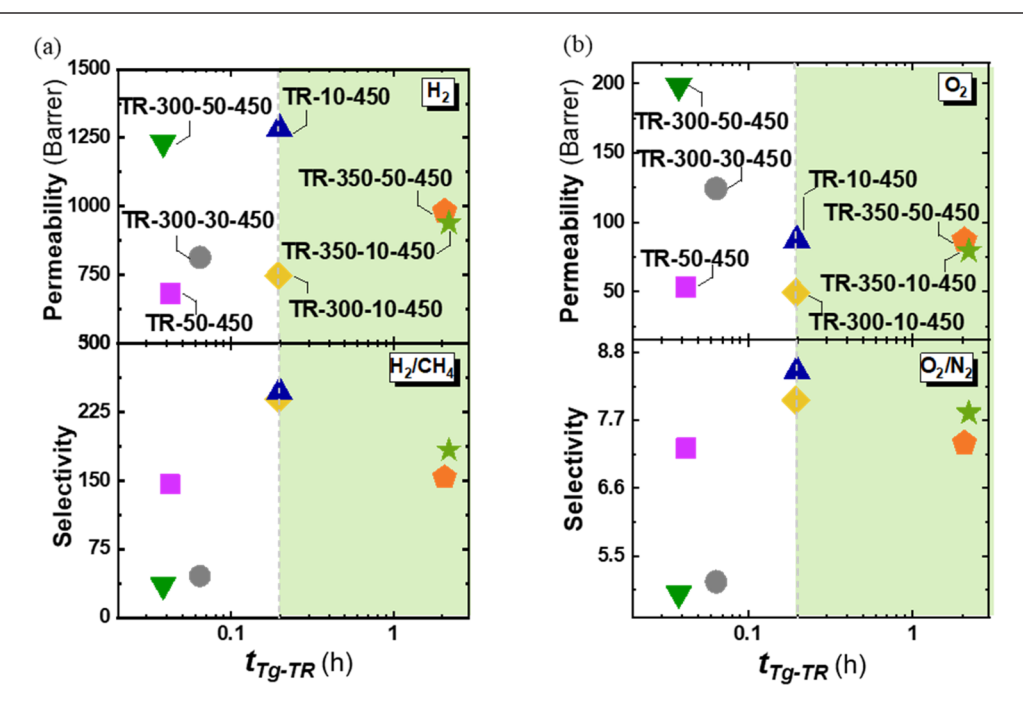


Figure 5. (a) H₂ permeability and H₂/CH₄ selectivity and (b) O₂ permeability and O₂/N₂ selectivity plotted against $t_{T_g\text{-TR}}$, defined as the exposure time of PPHI to temperatures above T_g (332 °C) and below T_{TR} (450 °C). The four PPBO films in the green-shaded region starting from $t_{T_g\text{-TR}}$ of 0.195 h (~12 min) performed beyond or closest to the most recent 2015 H₂/CH₄ and O₂/N₂ upper bounds.¹⁴

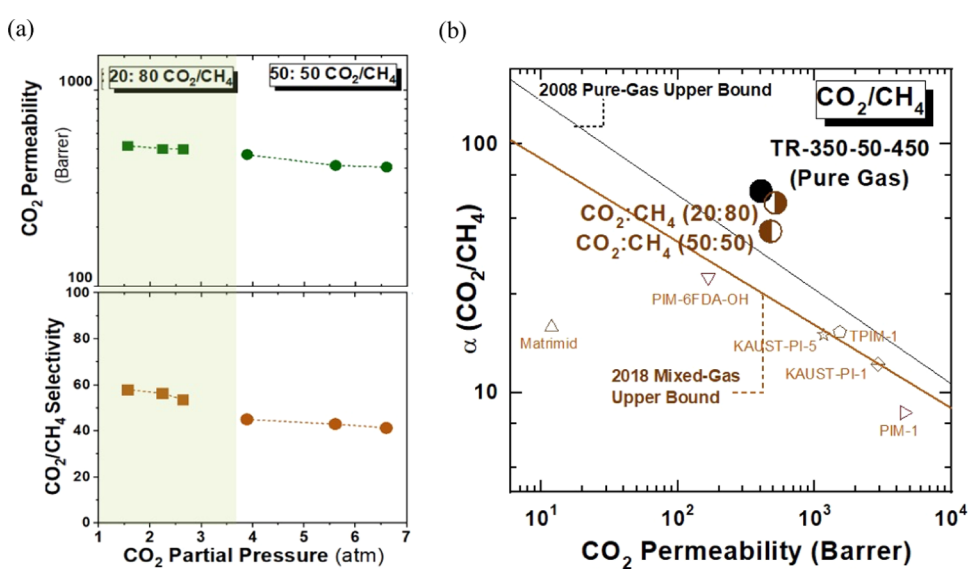


Figure 6. (a) CO₂ permeability and CO₂/CH₄ selectivity vs CO₂ partial pressures under two different feed compositions of 20:80 and 50:50 mole ratio CO₂/CH₄ mixed-gas feed; (b) CO₂/CH₄ upper-bound plot of the TR-350-50-450 PPBO film, where a black solid dot is the pure-gas permeation result and half-filled brown circles are mixed-gas permeation data with CO₂: CH₄ feed compositions in 20:80 and 50:50 relative to the mixed-gas upper bound⁷⁰ and highlighted the mixed-gas permeation results of PIM-1,⁷¹ Matrimid,⁷² TPIM-1,⁷³ KAUST-PI-1,⁷⁴ KAUST-PI-5,⁷⁴ and PIM-6FDA-OH.⁷⁵

thermal protocols as a function of $t_{T_o\text{-TR}}$ for H_2/CH_4 (Figure 5a), O_2/N_2 (Figure 5b), and CO_2/CH_4 separations (Figure S12) are achieved. It is noticeable that the four bestperforming (e.g., above the 2015 H₂/CH₄ upper bound) PPBO films, i.e., PPBO-300-10-450, PPBO-350-10-450, PPBO-350-50-450, and TR-10-450, are all exposed to above- $T_{\rm g}$ heat treatment with $t_{T_{\rm g}\text{-TR}}$ of at least 0.195 h (~12 min). This observation signifies that $t_{T_{a}\text{-TR}}$ of at least 12 min was able to activate the segmental motion to initialize TR and allow for the evolution of optimal microstructures achieving high permeability-selectivity combinations. As discussed above, the ultrahigh permeability of the four films was predominately contributed by the high diffusivity stemmed from their large fractional free volume (18.7-22.3%) and interchain distances (9.58-9.83 Å) due to the formation of large microcavities enabled by the sufficient above- $T_{\rm g}$ TR conversion. On the other hand, gas permeability showed a weak dependence on solubility, which may be due to the same nominal PPBO structure despite different TR protocols being applied. Nonetheless, small increments in the solubility of the more permeable penetrants were still observed in PPBOs with optimal $t_{T_{g}\text{-TR}}$ treatment. For example, the sorption of CO_2 enhanced by more than 10% as $t_{T_g\text{-TR}}$ increased from TR-50-450 (0.042 h) to TR-10-450 (0.198 h), which was potentially ascribed to the more available Langmuir sorption sites populated in the nonequilibrium free volume region associated with the higher FFV by TR-10-450.⁶⁸ The ultrahigh selectivity of the four films at $t_{T_g-TR} \ge 12$ min was largely facilitated by the diffusivity selectivity (i.e., size-sieving), which suggested the formation of narrow microcavity size distribution upon the optimal above- T_g TR conversion. For example, by dissociating the selectivity factor of O₂/N₂ gas pair (Figure S13a), diffusivity selectivity of the four best-performing films, in the range of 5.5-8.5, was significantly higher than those of the other three films (<5), which governed the overall sieving, given that the O2/N2 solubility selectivity of all PPBOs

experienced minor fluctuations between 1 and 2. For the CO₂/ CH₄ gas pair, solubility selectivity was the ruling sieving mechanism, originating from the sorption-controlled CO2 transport due to the strong dipole-quadrupole interaction between the polar CO2 molecule and the electron-rich PBO backbone (Figure S13b).^{28,69} However, the four films with more than 12 min above- T_g treatment exhibited substantial gain in CO2 diffusivity, such that the diffusivity selectivity became the more dominant sieving mechanism for their CO₂/ CH₄ separations at relatively well-maintained solubility selectivity. This further indicated that the films featured the TR characteristic hourglass-shape microstructures with the formation of large micropores interconnected by size-exclusive small microcavities, enabled by the optimal thermal treatment. Another observation is at $t_{T_g\text{-TR}}$ larger than 12 min; PPBOs with similar $t_{T_g\text{-TR}}$ shared similar selectivity, while when very long $t_{T_{\sigma}\text{-TR}}$ (>2 h) is applied, similar permeability was as well achieved. For example, H₂/CH₄ selectivity is almost identical for TR-300-10-450 and TR-10-450 films, both of which have a $t_{T_o\text{-TR}}$ of ~12 min; both gas permeabilities and selectivities align closely for TR-350-50-450 and TR-350-10-450 films, which share a similar $t_{T_{\sigma}\text{-TR}} > 2$ h. All of these results evidently showed that carefully controlled thermal protocols provide an instrumental approach to fine-tune the microporosity of TR PBO polymers, enabling superior gas separation performance to meet various challenging separation needs.

3.6. Mixed-Gas Permeation Tests and Physical Aging Study. CO₂ is known to induce an undesired plasticization effect in glassy polymers due to its high solubility and condensable nature. PPBO films did not show CO₂ plasticization up to 16 bar in pure-gas permeation tests (Figure S14). To further demonstrate plasticization resistance of PPBOs, mixed-gas CO₂/CH₄ separation performance was evaluated on the TR-350-50-450 film, one of the best-performing PPBO films. Natural gas wells usually contain up to 20% CO₂⁷⁵ to reflect PPBOs' potential for natural gas

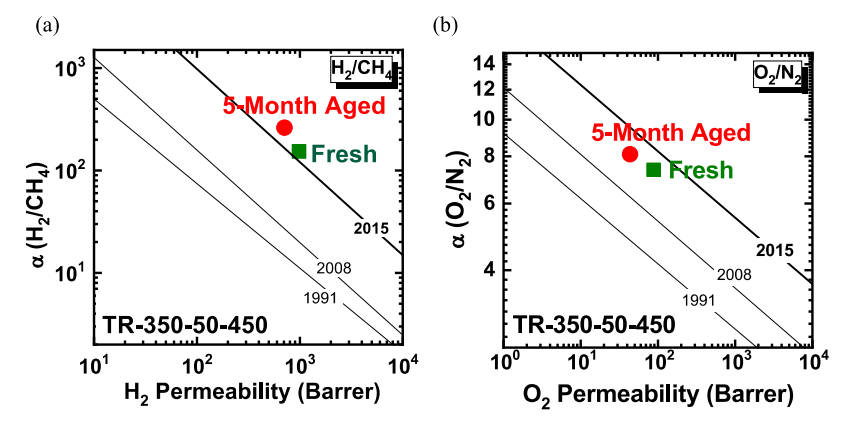


Figure 7. Upper-bound plots of the fresh and aged TR-350-50-450 PPBO films for separations of (a) H₂/CH₄ and (b) O₂/N₂.

sweetening applications; mixed-gas permeation tests were performed in two feed compositions, 20:80 and 50:50 CO₂/ CH₄ mol %, at CO₂ partial pressures from 1.5 to 6.6 bar. Partial pressure-dependent CO₂/CH₄ separation performance is shown in Figure 6. As shown, mixed-gas CO₂ permeability slightly decreased with increasing CO2 partial pressure, by which the monotonic decrease in permeability with increasing CO₂ fugacity indicates excellent plasticization resistance of the TR-350-50-450 film at a CO₂ partial pressure up to 6.6 atm at a 50:50 CO₂/CH₄ mol % mixed-gas feed (Figure 6a). A minor drop in mixed-gas CO₂/CH₄ selectivity at higher CO₂ partial pressure was observed due to a relatively larger decrease in CO₂ permeability than in CH₄ caused by the competitive sorption between CO₂ and CH₄, as commonly observed in glassy polymers. 76 Attributed to the rigid pentiptycene unit and its intrinsic size-sieving internal free volume, little change in mixed-gas CO₂ permeability from its pure-gas value was imposed while CH₄ permeability was effectively suppressed, which leveraged to the well-maintained mixed-gas selectivity, outperforming other TR PBOs where a drastic decrease of CO₂/CH₄ mixed-gas selectivity with pressure was commonly observed. \$1,77 As a result, the mixed-gas separation performance of TR-350-50-450 is far beyond the 2018 mixed-gas upper bound⁷⁰ (Figure 6b). In fact, the demonstration of plasticization resistance under much higher pressures and CO₂ contents is increasingly important as low CO2 content reservoirs are depleted, so the exploration of the current materials for such applications should be done; however, this is beyond the scope of this study.

Physical aging behavior was preliminarily investigated on the TR-350-50-450 film by measuring the pure-gas permeability after it had been aged for 5 months under ambient conditions. Physical aging, which involves polymer chain relaxation overtime to reach a thermodynamic equilibrium state with tighter chain packing, generally reduces permeability with some gains in selectivity.^{2,6} PPBO exhibited promising aging resistance with decently preserved permeability and marked enhanced selectivity upon aging (Figure 7), similar to other iptycene-containing polymers, such as iptycene-based polyimides,²⁹ triptycene-based PBOs,⁷⁸ and pentiptycene-based PIMs.²⁰ As shown, the 5 month aged TR-350-50-450 film maintained 72% H₂ permeability; at the same time, the H₂/ CH₄ selectivity of the aged sample exceeded the fresh film selectivity by 70%, moving the aged film even further beyond the 2015 H₂/CH₄ upper bound. Selective behavior was also observed for O₂/N₂, as shown in Figure 7b. Physical aging resistance of PPBOs originates from the configuration-based

and size-distinctive internal free volume elements intrinsic to the bulky pentiptycene units. In addition, interlocking between pentiptycene blades and chain threading also strengthened the interchain interactions, which effectively limited chain/segmental motion and thus provide excellent physical aging resistance.^{6,7}

4. CONCLUSIONS

An ortho-hydroxyl polyimide precursor incorporated with hierarchical pentiptycene (PPHI) was successfully prepared from a novel pentiptycene dianhydride monomer (PPDAn) and commercial 6FAP via solution imidization. Subsequent thermal rearrangement upon PPHI was carried out to afford a series of pentiptycene-based polybenzoxazole (PPBO) films by systematically varying two parameters of thermal protocols, i.e., T_g -dependent intermediate isotherm and the following heat rate to the final TR temperature. The individual effect of the two parameters suggested that the above- T_g isotherm and slow heating rate can each advance the permeability-selectivity performance in the correspondent PPBOs, potentially facilitated by the formation of an hourglass-like microstructure, enabling high gas throughput and especially size-sieving capability, which was allowed during the sufficient long treatment time at above $T_{\rm g}$ by essentially the synergistic contribution from the two parameters. As such, through the combination of engineered TR protocol and hierarchical molecular configuration of pentiptycene, PPBOs exceeded the latest trade-off upper bounds of several gas pairs. Moreover, the noncollapsible and size-specific nature of pentiptycene configuration and its intrinsic free volume elements led to excellent physical aging and plasticization resistance of PPBO, with minimal compromise from its pure-gas performance at the fresh state. Lastly, the fundamental insights in this study on performance optimization through $T_{\rm g}$ -dependent isotherm treatment could be potentially applied to other TR polymer systems.

ASSOCIATED CONTENT

Supporting Information

The Supporting Information is available free of charge at https://pubs.acs.org/doi/10.1021/acs.chemmater.1c04212.

Detailed information on NMR spectra of monomers; pictures of precursor PPHI polymer and films; pictures of PPBO films; FTIR spectra of PPBO films; O_2/N_2 separation performance of PPBO films reflecting heating rate effect; CO_2/CH_4 separation performance of PPBO

films reflecting heating rate effect; diffusivity coefficients as a function of the squared kinetic diameter of test gases; O_2/N_2 and CO_2/CH_4 separation performance of PPBO films reflecting intermediate temperature effect; pure-gas permeation results of all PPBO films relative to trade-off upper bounds; pure CO_2 permeabilities as a function of feed pressure; density, FFV, and d-spacing of PPBO films; pure-gas permeability and selectivity of PPBO films; and pure-gas diffusivity coefficients, solubility coefficients, diffusivity selectivity, and solubility selectivity of PPBO films (PDF)

AUTHOR INFORMATION

Corresponding Author

Ruilan Guo — Department of Chemical and Biomolecular Engineering, University of Notre Dame, Notre Dame, Indiana 46556, United States; orcid.org/0000-0002-3373-2588; Phone: 1-574-631-3453; Email: rguo@nd.edu; Fax: +1-574-631-8366

Authors

- Zihan Huang Department of Chemical and Biomolecular Engineering, University of Notre Dame, Notre Dame, Indiana 46556, United States
- Claire Yin Department of Chemical and Biomolecular Engineering, University of Notre Dame, Notre Dame, Indiana 46556, United States
- Tanner Corrado Department of Chemical and Biomolecular Engineering, University of Notre Dame, Notre Dame, Indiana 46556, United States
- Si Li Department of Chemical and Biomolecular Engineering, University of Notre Dame, Notre Dame, Indiana 46556, United States
- Qinnan Zhang Department of Chemical and Biomolecular Engineering, University of Notre Dame, Notre Dame, Indiana 46556, United States

Complete contact information is available at: https://pubs.acs.org/10.1021/acs.chemmater.1c04212

Author Contributions

The manuscript was written through the contributions of all authors. All authors have given approval to the final version of the manuscript.

Notes

The authors declare no competing financial interest.

ACKNOWLEDGMENTS

This work was supported by the National Science Foundation under Cooperative Agreement No. EEC-1647722 and the NSF ERC Center for Innovative and Strategic Transformation of Alkane Resources (CISTAR). Any opinions, findings, and conclusions or recommendations expressed in this material are those of the authors and do not necessarily reflect the views of the National Science Foundation. The authors gratefully acknowledge Professor Haiqing Lin and his lab at the University of Buffalo for use of their mixed-gas permeation cell to obtain the mixed-gas CO₂/CH₄ separation data. The Center for Environmental Science and Technology (CEST) at the University of Notre Dame is acknowledged for the use of characterization facilities.

REFERENCES

- (1) Baker, R. W.; Low, B. T. Gas Separation Membrane Materials: A Perspective. *Macromolecules* **2014**, *47*, 6999–7013.
- (2) Sanders, D. F.; Smith, Z. P.; Guo, R.; Robeson, L. M.; McGrath, J. E.; Paul, D. R.; Freeman, B. D. Energy-Efficient Polymeric Gas Separation Membranes for a Sustainable Future: A Review. *Polymer* **2013**, *54*, 4729–4761.
- (3) Bernardo, P.; Drioli, E.; Golemme, G. Membrane Gas Separation: A Review/State of the Art. *Ind. Eng. Chem. Res.* **2009**, 48, 4638–4663.
- (4) Sholl, D. S.; Lively, R. P. Seven Chemical Separations to Change the World. *Nature* **2016**, 532, 435–437.
- (5) Park, H. B.; Kamcev, J.; Robeson, L. M.; Elimelech, M.; Freeman, B. D. Maximizing the Right Stuff: The Trade-off between Membrane Permeability and Selectivity. *Science* **2017**, *356*, 1138–1148
- (6) Corrado, T.; Guo, R. Macromolecular Design Strategies toward Tailoring Free Volume in Glassy Polymers for High Performance Gas Separation Membranes. *Mol. Syst. Des. Eng.* **2020**, *5*, 22–48.
- (7) Weidman, J. R.; Guo, R. The Use of Iptycenes in Rational Macromolecular Design for Gas Separation Membrane Applications. *Ind. Eng. Chem. Res.* **2017**, *56*, 4220–4236.
- (8) Galizia, M.; Chi, W. S.; Smith, Z. P.; Merkel, T. C.; Baker, R. W.; Freeman, B. D. 50th Anniversary Perspective: Polymers and Mixed Matrix Membranes for Gas and Vapor Separation: A Review and Prospective Opportunities. *Macromolecules* **2017**, *50*, 7809–7843.
- (9) Robeson, L. M. The Upper Bound Revisited. *J. Membr. Sci.* **2008**, 320, 390–400.
- (10) Low, Z. X.; Budd, P. M.; McKeown, N. B.; Patterson, D. A. Gas Permeation Properties, Physical Aging, and Its Mitigation in High Free Volume Glassy Polymers. *Chem. Rev.* **2018**, *118*, 5871–5911.
- (11) El-Kaderi, H. M.; Hunt, J. R.; Mendoza-Cortés, J. L.; Côté, A. P.; Taylor, R. E.; O'Keeffe, M.; Yaghi, O. M. Designed Synthesis of 3D Covalent Organic Frameworks. *Science* **2007**, *316*, 268–272.
- (12) Carta, M.; Malpass-Evans, R.; Croad, M.; Rogan, Y.; Jansen, J. C.; Bernardo, P.; Bazzarelli, F.; McKeown, N. B. An Efficient Polymer Molecular Sieve for Membrane Gas Separations. *Science* **2013**, 339, 303–307.
- (13) Budd, P. M.; Elabas, E. S.; Ghanem, B. S.; Makhseed, S.; McKeown, N. B.; Msayib, K. J.; Tattershall, C. E.; Wang, D. Solution-Processed, Organophilic Membrane Derived from a Polymer of Intrinsic Microporosity. *Adv. Mater.* **2004**, *16*, 456–459.
- (14) Swaidan, R.; Ghanem, B.; Pinnau, I. Fine-Tuned Intrinsically Ultramicroporous Polymers Redefine the Permeability/Selectivity Upper Bounds of Membrane-Based Air and Hydrogen Separations. *ACS Macro Lett.* **2015**, *4*, 947–951.
- (15) Comesaña-Gándara, B.; Chen, J.; Bezzu, C. G.; Carta, M.; Rose, I.; Ferrari, M. C.; Esposito, E.; Fuoco, A.; Jansen, J. C.; McKeown, N. B. Redefining the Robeson Upper Bounds for CO2/CH4 and CO2/N2 Separations Using a Series of Ultrapermeable Benzotriptycene-Based Polymers of Intrinsic Microporosity. *Energy Environ. Sci.* **2019**, *12*, 2733–2740.
- (16) Park, H. B.; Jung, C. H.; Lee, Y. M.; Hill, A. J.; Pas, S. J.; Mudie, S. T.; Van Wagner, E.; Freeman, B. D.; Cookson, D. J. Polymers with Cavities Tuned for Fast Selective Transport of Small Molecules and Ions. *Science* **2007**, *318*, 254–258.
- (17) Kim, S.; Lee, Y. M. Rigid and Microporous Polymers for Gas Separation Membranes. *Prog. Polym. Sci.* **2015**, *43*, 1–32.
- (18) Park, H. B.; Han, S. H.; Jung, C. H.; Lee, Y. M.; Hill, A. J. Thermally Rearranged (TR) Polymer Membranes for CO2 Separation. J. Membr. Sci. 2010, 359, 11–24.
- (19) Robeson, L. M.; Dose, M. E.; Freeman, B. D.; Paul, D. R. Analysis of the Transport Properties of Thermally Rearranged (TR) Polymers and Polymers of Intrinsic Microporosity (PIM) Relative to Upper Bound Performance. *J. Membr. Sci.* **2017**, *525*, 18–24.
- (20) Corrado, T. J.; Huang, Z.; Huang, D.; Wamble, N.; Luo, T.; Guo, R. Pentiptycene-Based Ladder Polymers with Configurational Free Volume for Enhanced Gas Separation Performance and Physical

- Aging Resistance. *Proc. Natl. Acad. Sci. U.S.A.* **2021**, 118, No. e2022204118.
- (21) Luo, S.; Zhang, Q.; Zhu, L.; Lin, H.; Kazanowska, B. A.; Doherty, C. M.; Hill, A. J.; Gao, P.; Guo, R. Highly Selective and Permeable Microporous Polymer Membranes for Hydrogen Purification and CO2 Removal from Natural Gas. *Chem. Mater.* **2018**, *30*, 5322–5332.
- (22) Swaidan, R.; Ghanem, B.; Pinnau, I. Fine-Tuned Intrinsically Ultramicroporous Polymers Redefine the Permeability/Selectivity Upper Bounds of Membrane-Based Air and Hydrogen Separations. *ACS Macro Lett.* **2015**, *4*, 947–951.
- (23) Swager, T. M. Iptycenes in the Design of High Performance. Acc. Chem. Res. 2008, 41, 1181–1189.
- (24) Andrew, T. L.; Swager, T. M. Structure Property Relationships for Exciton Transfer in Conjugated Polymers. In *Nano-Optics for Enhancing Light-Matter Interactions on a Molecular Scale*; Springer Science + Business Media: Dordrecht, 2013; Vol. 100, pp 215–250.
- (25) Jiang, Y.; Chen, C. F. Recent Developments in Synthesis and Applications of Triptycene and Pentiptycene Derivatives. *Eur. J. Org. Chem.* **2011**, 2011, 6377–6403.
- (26) Chen, C.-F.; Ma, Y.-X. Iptycenes Chemistry: From Synthesis to Applications; Springer Science & Business Media, 2012; pp 3-5.
- (27) Luo, S.; Liu, Q.; Zhang, B.; Wiegand, J. R.; Freeman, B. D.; Guo, R. Pentiptycene-Based Polyimides with Hierarchically Controlled Molecular Cavity Architecture for Efficient Membrane Gas Separation. J. Membr. Sci. 2015, 480, 20–30.
- (28) Luo, S.; Liu, J.; Lin, H.; Kazanowska, B. A.; Hunckler, M. D.; Roeder, R. K.; Guo, R. Preparation and Gas Transport Properties of Triptycene-Containing Polybenzoxazole (PBO)-Based Polymers Derived from Thermal Rearrangement (TR) and Thermal Cyclodehydration (TC) Processes. J. Mater. Chem. A 2016, 4, 17050–17062
- (29) Luo, S.; Wiegand, J. R.; Gao, P.; Doherty, C. M.; Hill, A. J.; Guo, R. Molecular Origins of Fast and Selective Gas Transport in Pentiptycene-Containing Polyimide Membranes and Their Physical Aging Behavior. *J. Membr. Sci.* **2016**, *518*, 100–109.
- (30) Luo, S.; Wiegand, J. R.; Kazanowska, B.; Doherty, C. M.; Konstas, K.; Hill, A. J.; Guo, R. Finely Tuning the Free Volume Architecture in Iptycene-Containing Polyimides for Highly Selective and Fast Hydrogen Transport. *Macromolecules* **2016**, *49*, 3395–3405.
- (31) Yang, J. S.; Lee, C. C.; Yau, S. L.; Chang, C. C.; Lee, C. C.; Leu, J. M. Conformation and Monolayer Assembly Structure of a Pentiptycene-Derived α,ω -Alkanedithiol. *J. Org. Chem.* **2000**, *65*, 871–877.
- (32) Cao, J.; Lu, H. Y.; Chen, C. F. Synthesis, Structures, and Properties of Peripheral o-Dimethoxy-Substituted Pentiptycene Quinones and Their o-Quinone Derivatives. *Tetrahedron* **2009**, *65*, 8104–8112.
- (33) Bondi, A. van. Van Der Waals Volumes and Radii. J. Phys. Chem. A 1964, 68, 441-451.
- (34) Park, J.; Paul, D. R. Correlation and Prediction of Gas Permeability in Glassy Polymer Membrane Materials via a Modified Free Volume Based Group Contribution Method. *J. Membr. Sci.* **1997**, 125, 23–39.
- (35) Lin, H.; Freeman, B. D. Permeation and Diffusion. In *Springer-Handbook of Materials Measurement Methods*; Springer: New York, 2006; pp 371–387.
- (36) Calle, M.; Lozano, A. E.; Lee, Y. M. Formation of Thermally Rearranged (TR) Polybenzoxazoles: Effect of Synthesis Routes and Polymer Form. *Eur. Polym. J.* **2012**, *48*, 1313–1322.
- (37) Calle, M.; Chan, Y.; Jo, H. J.; Lee, Y. M. The Relationship between the Chemical Structure and Thermal Conversion Temperatures of Thermally Rearranged (TR) Polymers. *Polymer* **2012**, *53*, 2783–2791.
- (38) Luo, S.; Zhang, Q.; Bear, T. K.; Curtis, T. E.; Roeder, R. K.; Doherty, C. M.; Hill, A. J.; Guo, R. Triptycene-Containing Poly(Benzoxazole-Co-Imide) Membranes with Enhanced Mechanical Strength for High-Performance Gas Separation. *J. Membr. Sci.* **2018**, *551*, 305–314.

- (39) Guo, R.; Sanders, D. F.; Smith, Z. P.; Freeman, B. D.; Paul, D. R.; McGrath, J. E. Synthesis and Characterization of Thermally Rearranged (TR) Polymers: Influence of Ortho-Positioned Functional Groups of Polyimide Precursors on TR Process and Gas Transport Properties. J. Mater. Chem. A 2013, 1, 262–272.
- (40) Calle, M.; Chan, Y.; Jo, H. J.; Lee, Y. M. The Relationship between the Chemical Structure and Thermal Conversion Temperatures of Thermally Rearranged (TR) Polymers. *Polymer* **2012**, *53*, 2783–2791.
- (41) Sanders, D. F.; Smith, Z. P.; Ribeiro, C. P.; Guo, R.; McGrath, J. E.; Paul, D. R.; Freeman, B. D. Gas Permeability, Diffusivity, and Free Volume of Thermally Rearranged Polymers Based on 3,3′-Dihydroxy-4,4′-Diamino-Biphenyl (HAB) and 2,2′-Bis-(3,4-Dicarboxyphenyl) Hexafluoropropane Dianhydride (6FDA). *J. Membr. Sci.* 2012, 409–410, 232–241.
- (42) Li, S.; Jo, H. J.; Han, S. H.; Park, C. H.; Kim, S.; Budd, P. M.; Lee, Y. M. Mechanically Robust Thermally Rearranged (TR) Polymer Membranes with Spirobisindane for Gas Separation. *J. Membr. Sci.* **2013**, 434, 137–147.
- (43) Choi, J. I.; Jung, C. H.; Han, S. H.; Park, H. B.; Lee, Y. M. Thermally Rearranged (TR) Poly(Benzoxazole-Co-Pyrrolone) Membranes Tuned for High Gas Permeability and Selectivity. *J. Membr. Sci.* **2010**, 349, 358–368.
- (44) Moon, J. D.; Bridge, A. T.; D'Ambra, C.; Freeman, B. D.; Paul, D. R. Gas Separation Properties of Polybenzimidazole/Thermally-Rearranged Polymer Blends. *J. Membr. Sci.* **2019**, 582, 182–193.
- (45) Park, H. B.; Han, S. H.; Jung, C. H.; Lee, Y. M.; Hill, A. J. Thermally Rearranged (TR) Polymer Membranes for CO2 Separation. *J. Membr. Sci.* **2010**, 359, 11–24.
- (46) Wang, H.; Chung, T.-S. The Evolution of Physicochemical and Gas Transport Properties of Thermally Rearranged Polyhydroxyamide (PHA). *J. Membr. Sci.* **2011**, 385–386, 86–95.
- (47) Calle, M.; Chan, Y.; Jo, H. J.; Lee, Y. M. The Relationship between the Chemical Structure and Thermal Conversion Temperatures of Thermally Rearranged (TR) Polymers. *Polymer* **2012**, *53*, 2783–2791.
- (48) Han, S. H.; Misdan, N.; Kim, S.; Doherty, C. M.; Hill, A. J.; Lee, Y. M. Thermally Rearranged (TR) Polybenzoxazole: Effects of Diverse Imidization Routes on Physical Properties and Gas Transport Behaviors. *Macromolecules* **2010**, *43*, 7657–7667.
- (49) Han, S. H.; Kwon, H. J.; Kim, K. Y.; Seong, J. G.; Park, C. H.; Kim, S.; Doherty, C. M.; Thornton, A. W.; Hill, A. J.; Lozano, Á. E.; Berchtold, K. A.; Lee, Y. M. Tuning Microcavities in Thermally Rearranged Polymer Membranes for CO2 Capture. *Phys. Chem. Chem. Phys.* **2012**, *14*, 4365–4373.
- (50) Wang, M.; Wang, Z.; Li, S.; Zhang, C.; Wang, J.; Wang, S. A High Performance Antioxidative and Acid Resistant Membrane Prepared by Interfacial Polymerization for CO 2 Separation from Flue Gas. *Energy Environ. Sci.* **2013**, *6*, 539–551.
- (51) Calle, M.; Jo, H. J.; Doherty, C. M.; Hill, A. J.; Lee, Y. M. Cross-Linked Thermally Rearranged Poly(Benzoxazole-Co-Imide) Membranes Prepared from Ortho-Hydroxycopolyimides Containing Pendant Carboxyl Groups and Gas Separation Properties. *Macromolecules* **2015**, *48*, 2603–2613.
- (52) Soo, C. Y.; Jo, H. J.; Lee, Y. M.; Quay, J. R.; Murphy, M. K. Effect of the Chemical Structure of Various Diamines on the Gas Separation of Thermally Rearranged Poly(Benzoxazole-Co-Imide) (TR-PBO-Co-I) Membranes. *J. Membr. Sci.* **2013**, 444, 365–377.
- (53) Zhuang, Y.; Seong, J. G.; Lee, W. H.; Do, Y. S.; Lee, M. J.; Wang, G.; Guiver, M. D.; Lee, Y. M. Mechanically Tough, Thermally Rearranged (TR) Random/Block Poly(Benzoxazole-Co-Imide) Gas Separation Membranes. *Macromolecules* **2015**, *48*, 5286–5299.
- (54) Sanders, D. F.; Smith, Z. P.; Ribeiro, C. P.; Guo, R.; McGrath, J. E.; Paul, D. R.; Freeman, B. D. Gas Permeability, Diffusivity, and Free Volume of Thermally Rearranged Polymers Based on 3,3′-Dihydroxy-4,4′-Diamino-Biphenyl (HAB) and 2,2′-Bis-(3,4-Dicarboxyphenyl) Hexafluoropropane Dianhydride (6FDA). *J. Membr. Sci.* 2012, 409–410, 232–241.

- (55) Li, S.; Jo, H. J.; Han, S. H.; Park, C. H.; Kim, S.; Budd, P. M.; Lee, Y. M. Mechanically Robust Thermally Rearranged (TR) Polymer Membranes with Spirobisindane for Gas Separation. *J. Membr. Sci.* **2013**, 434, 137–147.
- (56) Shamsipur, H.; Dawood, B. A.; Budd, P. M.; Bernardo, P.; Clarizia, G.; Jansen, J. C. Thermally Rearrangeable PIM-Polyimides for Gas Separation Membranes. *Macromolecules* **2014**, *47*, 5595–5606.
- (57) Zhang, Y.; Musselman, I. H.; Ferraris, J. P.; Balkus, K. J. Gas Permeability Properties of Matrimid Membranes Containing the Metal-Organic Framework Cu-BPY-HFS. *J. Membr. Sci.* **2008**, 313, 170–181.
- (58) Aitken, C. L.; Koros, W. J.; Paul, D. R. Effect of Structural Symmetry on Gas Transport Properties of Polysulfones. *Macromolecules* **1992**, 25, 3424–3434.
- (59) Puleo, A. C.; Paul, D. R.; Kelley, S. S. The Effect of Degree of Acetylation on Gas Sorption and Transport Behavior in Cellulose Acetate. *J. Membr. Sci.* **1989**, *47*, 301–332.
- (60) Budd, P. M.; Msayib, K. J.; Tattershall, C. E.; Ghanem, B. S.; Reynolds, K. J.; McKeown, N. B.; Fritsch, D. Gas Separation Membranes from Polymers of Intrinsic Microporosity. *J. Membr. Sci.* **2005**, *251*, *263*–*269*.
- (61) Carta, M.; Croad, M.; Malpass-Evans, R.; Jansen, J. C.; Bernardo, P.; Clarizia, G.; Friess, K.; Lanč, M.; McKeown, N. B. Triptycene Induced Enhancement of Membrane Gas Selectivity for Microporous Tröger's Base Polymers. *Adv. Mater.* **2014**, *26*, 3526–3531.
- (62) Ghanem, B. S.; Swaidan, R.; Litwiller, E.; Pinnau, I. Ultra-Microporous Triptycene-Based Polyimide Membranes for High-Performance Gas Separation. *Adv. Mater.* **2014**, *26*, 3688–3692.
- (63) Ghanem, B. S.; Swaidan, R.; Ma, X.; Litwiller, E.; Pinnau, I. Energy-Efficient Hydrogen Separation by AB-Type Ladder-Polymer Molecular Sieves. *Adv. Mater.* **2014**, *26*, 6696–6700.
- (64) Ye, L.; Wang, L.; Jie, X.; Yu, C.; Kang, G.; Cao, Y. The Evolution of Free Volume and Gas Transport Properties for the Thermal Rearrangement of Poly(Hydroxyamide-Co-Amide)s Membranes. *J. Membr. Sci.* **2019**, *573*, 21–35.
- (65) Park, H. B.; Jung, C. H.; Lee, Y. M.; Hill, A. J.; Pas, S. J.; Mudie, S. T.; Van Wagner, E.; Freeman, B. D.; Cookson, D. J. Polymers with Cavities Tuned for Fast Selective Transport of Small Molecules and Ions. *Science* **2007**, *318*, 254–258.
- (66) Koros, W. J.; Fleming, G. K. Membrane-Based Gas Separation. J. Membr. Sci. 1993, 83, 1–80.
- (67) Iyer, G.; Liu, L.; Zhang, C. Hydrocarbon Separations by Glassy Polymer Membranes. *J. Polym. Sci.* **2020**, *58*, 2482–2517.
- (68) Matteucci, S.; Yampolskii, Y.; Freeman, B. D.; Pinnau, I. Transport of Gases and Vapors in Glassy and Rubbery Polymers. In *Materials Science of Membranes for Gas and Vapor Separation*; John Wiley & Sons, Ltd, 2006; pp 1–47.
- (69) Patel, H. A.; Ko, D.; Yavuz, C. T. Nanoporous Benzoxazole Networks by Silylated Monomers, Their Exceptional Thermal Stability, and Carbon Dioxide Capture Capacity. *Chem. Mater.* **2014**, *26*, 6729–6733.
- (70) Wang, Y.; Ma, X.; Ghanem, B. S.; Alghunaimi, F.; Pinnau, I.; Han, Y. Polymers of Intrinsic Microporosity for Energy-Intensive Membrane-Based Gas Separations. *Mater. Today Nano* **2018**, *3*, 69–95.
- (71) Swaidan, R.; Ghanem, B. S.; Litwiller, E.; Pinnau, I. Pure- and Mixed-Gas CO2/CH4 Separation Properties of PIM-1 and an Amidoxime-Functionalized PIM-1. *J. Membr. Sci.* **2014**, *487*, 95–102.
- (72) Tin, P. S.; Chung, T. S.; Liu, Y.; Wang, R.; Liu, S. L.; Pramoda, P.; et al. Effects of Cross-Linking Modification on Gas Separation performance of Matrimid Membranes. *J. Membr. Sci.* **2003**, *225*, 77–79.
- (73) Swaidan, R.; Ghanem, B.; Litwiller, E.; Pinnau, I. Physical Aging, Plasticization and Their Effects on Gas Permeation in "Rigid" Polymers of Intrinsic Microporosity. *Macromolecules* **2015**, *48*, 6553–6561.

- (74) Swaidan, R.; Ghanem, B.; Al-Saeedi, M.; Litwiller, E.; Pinnau, I. Role of Intrachain Rigidity in the Plasticization of Intrinsically Microporous Triptycene-Based Polyimide Membranes in Mixed-Gas CO 2 /CH 4 Separations. *Macromolecules* **2014**, *47*, 7453–7462.
- (75) Ma, X.; Swaidan, R.; Belmabkhout, Y.; Zhu, Y.; Litwiller, E.; Jouiad, M.; Pinnau, I.; Han, Y. Synthesis and Gas Transport Properties of Hydroxyl-Functionalized Polyimides with Intrinsic Microporosity. *Macromolecules* **2012**, *45*, 3841–3849.
- (76) Visser, T.; Masetto, N.; Wessling, M. Materials Dependence of Mixed Gas Plasticization Behavior in Asymmetric Membranes. *J. Membr. Sci.* **2007**, 306, 16–28.
- (77) Shao, L.; Chung, T. S.; Goh, S. H.; Pramoda, K. P. Polyimide Modification by a Linear Aliphatic Diamine to Enhance Transport Performance and Plasticization Resistance. *J. Membr. Sci.* **2005**, *256*, 46–56.
- (78) Crist, R. D.; Huang, Z.; Guo, R.; Galizia, M. Effect of Thermal Treatment on the Structure and Gas Transport Properties of a Triptycene-Based Polybenzoxazole Exhibiting Configurational Free Volume. *J. Membr. Sci.* **2020**, 597, No. 117759.

□ Recommended by ACS

Fabrication of Swellable Organic–Inorganic Hybrid Polymers for CO₂-Assisted Hydration of Propylene Epoxide

Lulu Dang, Guohua Gao, et al.

MARCH 20, 2023

ACS APPLIED MATERIALS & INTERFACES

READ 🗹

Hyper-Cross-Linked Polymers with Sulfur-Based Functionalities for the Prevention of Aging Effects in PIM-1 Mixed Matrix Membranes

Federico Begni, Maria-Chiara Ferrari, et al.

MAY 25, 2023

ACS APPLIED POLYMER MATERIALS

READ 🗹

Pentiptycene-Containing Polybenzoxazole Membranes with a Crosslinked Unimodal Network Structure for High-Temperature Hydrogen Separations

Si Li, Ruilan Guo, et al.

OCTOBER 26, 2022

CHEMISTRY OF MATERIALS

READ 🗹

Synthesis and Gas Separation Properties of Aromatic Polyimides Containing Noncoplanar Rigid Sites

Xiaohua Tong, Chunhai Chen, et al.

AUGUST 03, 2022

ACS APPLIED POLYMER MATERIALS

READ 🗹

Get More Suggestions >